FORMATION OF TIP VORTICES AND VORTEX WAKE ALLEVIATION BY TIP DEVICES

ICAS-90-3.2.2

R. Staufenbiel and T. Vitting

Department of Aerospace Engineering
RWTH Aachen, University of Technology
5100 Aachen, Federal Republic of Germany

Abstract

Formation and structure of wing tip vortices as well as some methods of vortex wake alleviation are subject of the paper. The formation of vortices is investigated theoretically and experimentally. For calculating the roll-up of vortices, a modified line vortex method is introduced using an amalgamation process which preserves important conservation laws. A comparison of experimental and theoretical data yields good agreement. In the second part of the paper, different ways of tip vortex dissipation have been tested such as destabilization of vortices, stimulation of vortex breakdown and redistribution of the vorticity in tip vortices. Experiments, carried out in a water tunnel, evaluated vortex structure as well as profiles of tangential and axial velocity components using LDV and flow visualization techniques.

Introduction

The vortices generated by large aircraft can present a severe hazard to other aircraft which inadvertently encounter the vortices. To prevent aircraft-vortex encounters, the separation standards behind heavy jets have been increased. Airport utilization is projected to double by the end of this century. Runway capacity cannot be increased until the wake vortex problem has been alleviated.

A lot of papers have been published on the formation of wing wakes [1..6], but it cannot yet be claimed that the initial roll-up process is fully understood. Since control of vortices depends upon understanding of the birth process of a vortex, a first part of the paper is concerned with the formation and the structure of tip vortices. For this purpose, a modified line vortex method has been developed to model the time-dependent distribution of vorticity in tip vortices during the roll-up process. This method is based on a special amalgamation procedure which preserves important conservation laws. Predictions from the computational method have been compared to experimental results, obtained in a water tunnel, showing good correlation to some basic results of the theory. On the base of these theoretical and experimental studies, several ways to reduce the hazard of wing wakes have been studied theoretically and experimentally.

Control of vortices aims to a reduction in vortex strength and to dissipation of trailing vortices which should happen more rapidly than the natural ageing process. Vortex control can mainly be effected by

- — modifying the lift distribution
- — stimulating vortex instability and breakdown
- — spreading vorticity by splitting the vorticity into more than one concentrated vortex
- — preventing an ordered roll-up process

The paper presents some examples for the first three control mechanisms. To be successful in controlling vortices, it is mandatory to understand vortex formation and structu depending on lift distribution. This subject is discussed in the first part of the paper while the methods of vortex control are presented in the second part.

Nomenclature

a	=	radius of the stator
A	=	parameter in the vortex model
AR	=	aspect ratio
C_{Di}	=	induced drag coefficient
C_L	=	wing lift coefficient
$\hat{c}_{po}$	=	pressure cofficient at the vortex center, (Eq. 9)
D_i	=	induced drag
ΔH	=	loss in total pressure
R	=	radial distance from the vortex center
s	=	halfspan of the wing
S	=	wing area
t	=	time
V_∞	=	inflow velocity
V	=	flow velocity
V	=	dimensionless velocity ($=Vs/\Gamma_0$)
x,y,z	=	streamwise, spanwise, and wing normal coordinates
α	=	angle of attack
β	=	scale factor in Eq.7
γ	=	circulation of a single line vortex, in units of Γ_0
Γ_0	=	circulation in the wing plane of symmetry
ρ	=	air density
τ	=	dimensionless time $=(t\,\Gamma_0/s^2)$

Indices

a	=	axial component
am	=	amalgamated
c	=	vortex core
l_∞	=	local free-stream
i	=	inner part of the amalgamated vortex
o	=	outer part of the amalgamated vortex
s	=	stator
t	=	tangential component

The formation of tip vortices

The Biot-Savart Approach

Trailing vortices are formed if the shear layer shed from a wing rolls up into regions of high vorticity. Around the centers of vorticity the tangential velocities increase up to a maximum

value at the radius of the so called vortex core. Within this regime about 50% to 70% of the wing wake vorticity is concentrated. Following an analysis of Spreiter and Sacks [6], the rate of formation of rotational energy in the wake induced by the trailing vortices is directly related to the induced drag.

$$D_i = \frac{1}{2}\rho V_\infty^2 C_{Di} S = \iint \frac{1}{2}\rho V_t^2 \, dA \qquad (1)$$

where the integral is performed over the entire plane normal to the flight direction.

If the trailing-vortex sheet of a wing is represented by an array of line vortices (n vortices per half wing with the strength γ_i), then the motion of the line vortices and, thus, the roll-up process can be calculated by solving 2n first order ordinary differential equations, the Biot-Savart equations:

$$\frac{dy_i}{dt} = -\sum_{j\neq i} \frac{1}{2\pi} \gamma_j \frac{z_i - z_j}{(y_i - y_j)^2 + (z_i - z_j)^2}$$

$$\frac{dz_i}{dt} = \sum_{j\neq i} \frac{1}{2\pi} \gamma_j \frac{y_i - y_j}{(y_i - y_j)^2 + (z_i - z_j)^2} \qquad (2)$$

The Biot-Savart approach leads to two difficulties. First, the vortex filaments are singularities and create large velocities in their neighborhood. This causes instabilities and sheet crossings during roll-up in a chaotic manner. The second difficulty concerns the CPU time. The number of operations is proportional to n^2 and CPU time increases, if more line vortices are chosen for a better representation of the vortex sheet.

In spite of the chaotic motion, the Biot-Savart approach meets some important conservation laws, as can easily be derived from Eq. (2). The energy induced by the vortical flow field, the center of vorticity (for each half wing), and the second moment of vorticity distribution (for likesign vorticity) are conserved [7,8]. The conservation of energy is equivalent to the time-invariance of the Kirchhoff-Routh function :

$$K = \frac{1}{2\pi} \sum_{i<j} \gamma_i \gamma_j \ln (r_{ij}/s) \qquad (3)$$

where r_{ij} is the relative distance between the line vortices i and j. The Kirchhoff-Routh function is very useful because it is directly related to the induced drag, if the number of line vortices is large enough:

$$-K \rightarrow D_i/\rho \qquad (4)$$

The roll-up process will be described by a modified line vortex approach in which a special amalgamation process is used. Amalgamation is a known method with a number of positive effects [9]. It can be used to limit the large velocities induced near line vortices, to simulate some naturally occurring merging of vorticity and to reduce the computer time.

It has been customary to amalgamate two or more vortices into a single vortex of the strength $\Sigma\gamma_i$, placed at their center of vorticity. This process only conserves the total circulation and the center of vorticity; the second moment of vorticity distribution and, in particular, the energy decrease. Hence, an amalgamation procedure has been developed which, in addition to the total circulation and the center of vorticity, also conserves energy and second moment. In the following, the vortex dynamics — given by vortex position, time and velocity components — are described in dimensionless units

$$y/s; \quad z/s; \quad \tau = \frac{t\Gamma_0}{s^2}; \quad \bar{V}_t = \frac{V_t s}{\Gamma_0}$$

where Γ_0 and s are the maximum circulation and the halfspan of the wing respectively. The advantage of these definitions follows directly from the Biot-Savart equations.

A modified line vortex method

In this section a computational method is presented which is based upon a special amalgamation process. When a sheet crossing develops, the amalgamation is performed in such a way, that a structured, concentrated vortex is fed. The vorticity of the concentrated vortex is distributed so that the circulation corresponds to a modified Lamb-Oseen model

$$\Gamma = \Gamma_{am} \left[A + (1-A)R/R_0\right]\left[1 - e^{-(R/R_i)^2}\right] \qquad (5)$$

Three time-dependent parameters are incorporated in the model, Γ_{am}, R_i and R_o. The parameter A has a smaller influence on the results and was chosen as constant, A=0.7, [7]. The term in the second bracket describes the well-known Lamb-Oseen model, and by adapting the "inner radius" R_i — which is approximately equal to the core radius R_c, ($R_c/R_i \approx 1.1$) — at each amalgamation step it is possible to conserve the energy, given by Eq. (3), while the term in the first bracket permits to conserve the second moment of vorticity distribution by adapting the "outer radius" R_o. Γ_{am} is the momentary circulation of the amalgamated vortex. Details of this amalgamation and restructuring process are given in [10].

The equations of motion, Eq. (2), were integrated by a fourth-order Runge-Kutta integration scheme using a constant dimensionless timestep of $\Delta\tau = 10^{-4}$ and carried out with a precision of sixteen decimal digits. The vortex sheet was discretized by a suitable arrangement of 200 line vortices with constant strength, γ_i=const. Each vortex filament was positioned in the center of the portion of vorticity represented by line vortex strength γ_i.

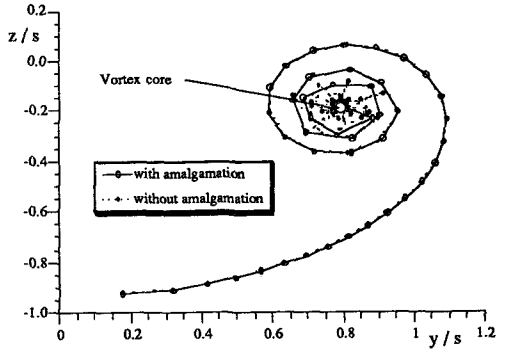

Fig. 1 Positions of line vortices at τ=2.5

Fig. 1 compares the vortex sheets generated by a wing with elliptical lift distribution at dimensionless time of τ=2.5 with and without amalgamation. Also the tangential velocity profile

was computed for the same configuration (Fig. 2). At this time 60% of the vorticity has been amalgamated but only 25% is concentrated within the vortex core of $R_i/s=0.015$. The larger part of the vorticity is spread around the core, up to a radius of $R_o/s=0.14$, so that the second moment of vorticity distribution is conserved. A similar, but chaotic spreading of the vorticity can be observed from the results without amalgamation, as shown in Fig. 1.

The duration of the complete roll-up process for the elliptical lift distribution can be taken from Fig. 3 and 4. These diagrams show the radii of the inner and outer region as a function of dimensionless time. The inner radius increases to about 0.05 of the halfspan, while the radius of the outer region grows up to about 0.68 of the halfspan.

Fig. 5 shows the maximum tangential velocity versus time. The maximum of the tangential velocity starts from a high value and ends up with a dimensionless value of about 1.4. Hence, the maximum tangential velocity decreases with time until the roll-up process is finished without assuming that an ageing process under the influence of viscosity is present. This result is not obvious considering the fact that the vorticity in the vortex core increases during the roll-up process. But, the conservation of energy requires that the core radius grows faster than the core vorticity.

The circulation Γ_{am} of the amalgamated vortex is plotted in Fig. 6 as function of time. It reveals a fast increase at the beginning of the roll-up. For elliptical lift distribution the roll-up process requires a dimensionless time of about $\tau=30$. During this time the parameters of the amalgamated vortex grow. Now, the dimensionless time is equivalent to a distance behind the wing in units of half span

$$\frac{x}{s}=\tau/\left(\frac{\Gamma_0}{s\,V_\infty}\right) \tag{6}$$

where the scale factor may be expressed in terms of lift coefficient and aspect ratio

$$\left(\frac{\Gamma_0}{V_\infty s}\right)=\beta\left(\frac{4\,C_L}{\pi\,AR}\right) \tag{7}$$

where β depends on the lift distribution, with $\beta=1$ for an elliptical lift distribution.

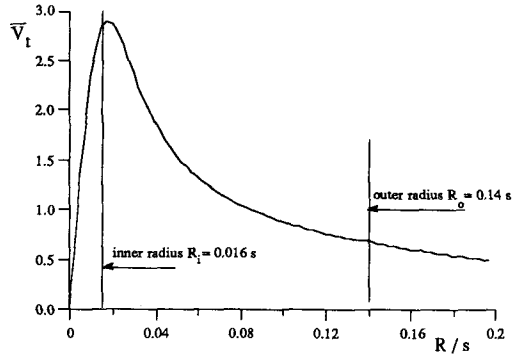

Fig. 2 Tangential velocity profile at $\tau=2.5$

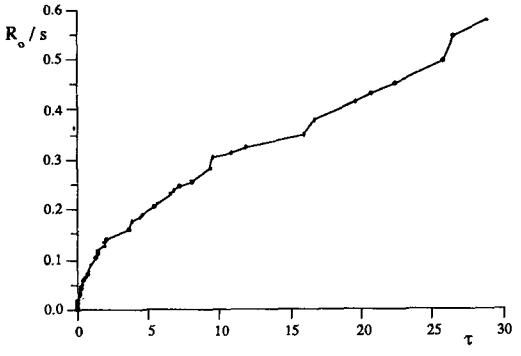

Fig. 4 Outer radius of the amalgamated vortex

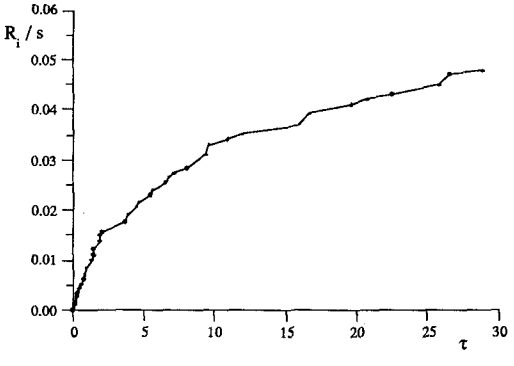

Fig. 3 Inner radius of the amalgamated vortex

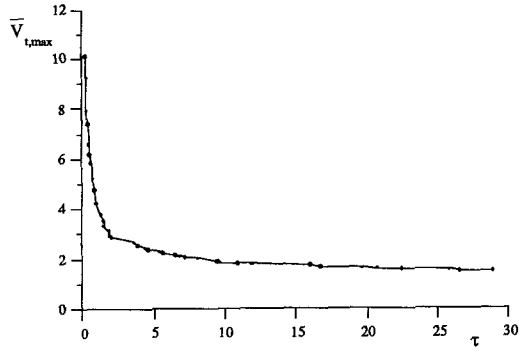

Fig. 5 Maximum dimensionsless tangential velocity

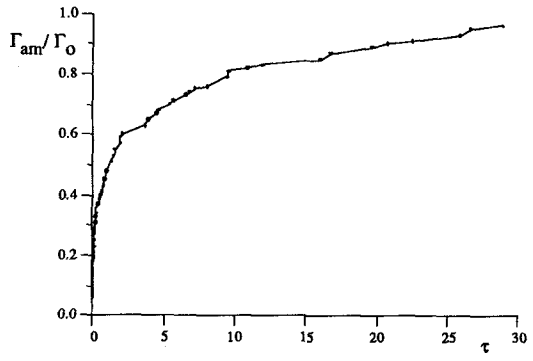

Fig. 6 Circulation of the amalgamated vortex

Thus, Eq. (6) can be written as

$$\frac{x}{s} = \frac{\pi\, AR}{4\,\beta\, C_L}\,\tau \qquad (8)$$

Specifying a lift coefficient of C_L=1 and an aspect ratio of 8, the roll-up is finished not before a distance of about 180 half spans or 720 mean chords. Over such a distance the viscosity cannot be neglected any longer, and it is almost impossible to perform measurements in wind or water tunnels.

Still another interesting fact can be derived from the numerical results. As long as the roll-up process has not been terminated, the static pressure at the center of the vortex increases thereby reducing the axial velocity in the vortex core. Using the model of Eq. (5) with parameters known as function of time, the static pressure at the vortex center can be calculated from

$$\frac{p_0 - p_\infty}{\rho} = \int_\infty^0 \frac{\Gamma^2}{r^3}\,dr \qquad (9)$$

For an elliptical lift distribution, the result of this evaluation is shown as pressure coefficient depending on dimensionless time τ in Fig. 7, where a special pressure coefficient is introduced :

$$\hat{c}_{p0} = \frac{p_0 - p_\infty}{\rho/2\,(\Gamma_0/s)^2} \qquad (10)$$

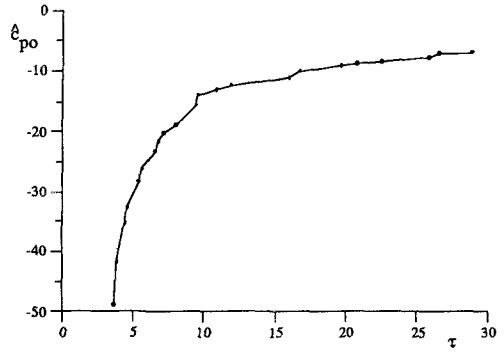

Fig. 7 Pressure coefficient at the vortex center

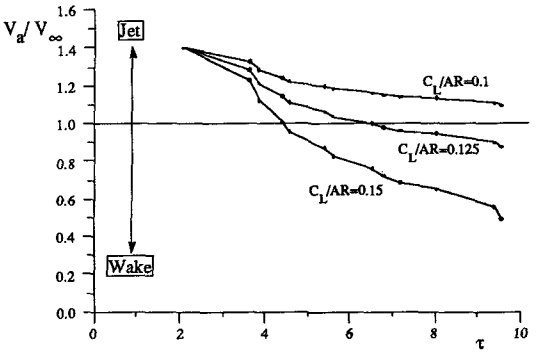

Fig. 8 Axial velocity at the vortex center

Then, the axial velocity at the vortex center can be obtained as function of time from the relation

$$\left(\frac{V_a}{V_\infty}\right)^2 = 1 - \hat{c}_{p0}(\tau)\left(\frac{\Gamma_0}{V_\infty s}\right)^2 - \Delta H \qquad (11)$$

where ΔH is the loss in total pressure. If an initial value of the axial velocity is given — e.g., taken from experiments —, and ΔH is assumed as approximately time-independent, the time-dependent axial velocity is related to the pressure coefficients

$$\left(\frac{V_a}{V_\infty}\right)^2 = \left(\frac{V_{a0}}{V_\infty}\right)^2 - \left[\hat{c}_{p0}(\tau) - \hat{c}_{p0}(\tau_0)\right]\left(\frac{\Gamma_0}{V_\infty s}\right)^2 \qquad (12)$$

Substituting Eq. (7) into Eq. (11) leads to results, evaluated for an initial value of V_{a0}=1.4 (jet type), illustrated in Fig. 8 for three values of (C_L/AR). The defect in axial velocity increases with growing values of (C_L/AR).

Roll-up past rectangular wing planforms

As shown above for an elliptical lift distribution, the rolling up of the vortex sheet to concentrated tip vortices requires several hundred chord lengths. Now, one might suppose that the rolling up can be accelerated distinctly by concentrating the vorticity on a smaller part of the outer wing. Such a higher concentration of vorticity can be realized by using rectangular wing planforms.

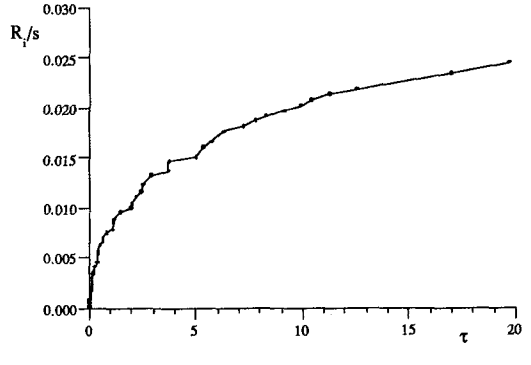

Fig. 9 Development of R_i for a rectangular planform (AR=4)

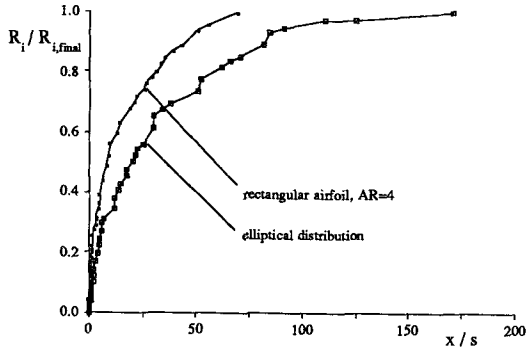

Fig. 10 Development of R_i for elliptical distribution and rectangular planform (AR=4)

Using the modified line vortex method, the simulation of the roll-up process was performed for a rectangular wing with an aspect ratio of 4. Fig. 9 shows the inner radius of the amalgamated vortex as a function of the dimensionless time τ and in Fig. 10 is shown, that the roll-up process can be accelerated in this case by a factor of 3 compared to an elliptical lift distribution with the same value of $C_L/AR=0.25$.

As another result of the simulations, the maximum tangential velocities are compared (Fig. 11). In both cases the dimensionless tangential velocities decrease during the roll-up down to constant values, which differ by a factor of 2, the value for the rectangular planform being the larger one. Numerical investigations, based on the amalgamation method, have been performed for various lift distributions (parabolic and elliptical) and for rectangular planform with various aspect ratios. In Fig. 12, results are given for the final maximum tangential velocity.

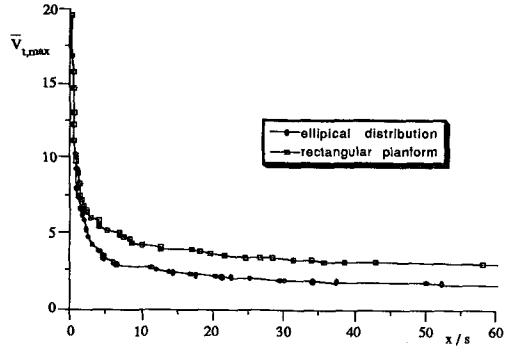

Fig. 11 Maximum tangential velocities for elliptical distribution and rectangular planform (AR=4)

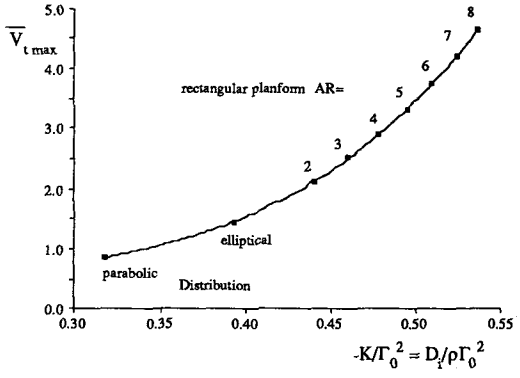

Fig. 12 Maximum tangential velocities for various lift distributions

It was found, that the dimensionless velocity depends smoothly on the normalized Kirchhoff-Routh function

$$-\frac{K}{\Gamma_0^2} = \frac{D_i}{\rho\,\Gamma_0^2} \qquad (13)$$

The experiments, described in the following section, use rectangular wing planforms for two reasons: the roll-up is faster, variations of the aspect ratio are very easy to realize.

Experimental validation of the modified line vortex method

Experimental setup

Experiments for the validation of the modified line vortex method were carried out mainly in a "Goettingen Type" water-tunnel with a cross-section of 0.53m * 0.53m and a section length of 1m. The Reynolds numbers, using the wing chord as reference length, varied from 50000 to 200000. To visualize the flow characteristics, little hydrogen bubbles have been produced by an electrolysis process. Gas bubbles are quite suitable to make the center of a vortex visible as there exists a pressure minimum at the vortex center which leads to hydrostatic forces. Velocity measurements were performed by a two-component Argon-LDV in back-scattering mode. With this setup it was possible to measure the free-stream direction and normal to the wing planform. To obtain correct results of the tangential velocity profile of a vortex, it was necessary to direct the LDV measuring volume in such a way that the axis of the vortex was met. Hence, flow visualization and LDV-measurements had to be combined to adjust the measuring volume correctly.

All wings used for the generation of tip vortices had a rectangular planform and a Clark-Y profile as cross-section. If not stated otherwise, the wing tip was rounded out to obtain chordwise a half-circle cross-section at the tip. The chord length varied from 0.045m to 0.155m and the span from 0.115m to 0.4m. By this variation aspect ratios from 1.5 up to 10 could be realized.

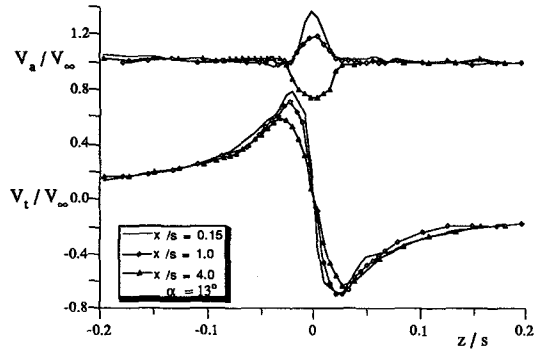

Fig. 13 Axial and tangential velocities as function of distance

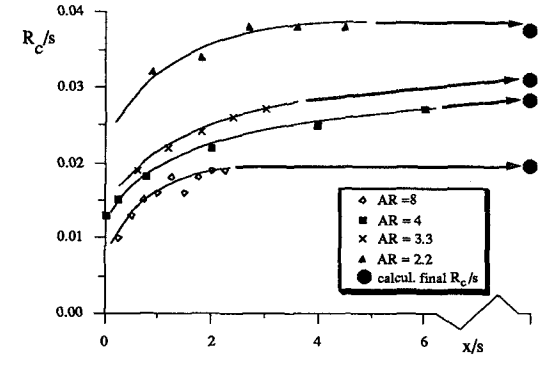

Fig.14 Core radius as function of distance for various aspect ratios

Results

The Fig. 13 shows axial and tangential velocity profiles at three different stations behind the wing. These principal tendencies of the results agree well with the those predicted by the simulations:

— the maximum tangential velocity V_t decreases with downstream distance,
— the core radius R_c grows and
— the axial velocity V_a at the vortex center decreases.

For a quantitative comparison between simulations and experiments, Fig.14 shows the core radius as function of the distance x/s for various values of the aspect ratio. As predicted by the computations, R_c/s increases with x/s and a saturation can be observed for about $x/s \geq 5$. The final value of the core radius decreases with growing aspect ratio. The calculated final core radii are plotted at the right hand border of the diagram for corresponding aspect ratios. The calculated final values of R_c/s agree well with the experimental data of R_c/s.

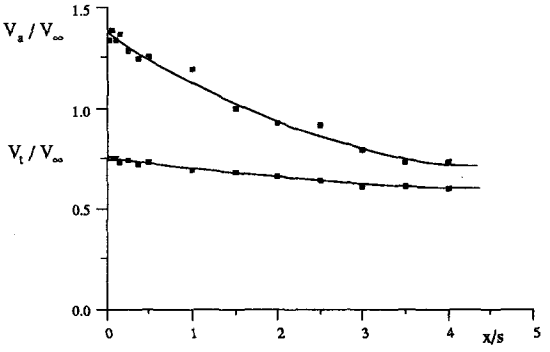

Fig.15 Axial velocity and tangential velocities as function of distance

Different to the calculated values, the measured velocity components are expressed in units of the free-stream value. These dimensionless terms are related to $\bar{V}_t$, above defined, by

$$\frac{V_t}{V_\infty} = \bar{V}_t \frac{\Gamma_0}{s\, V_\infty} = \bar{V}_t \beta \frac{4 C_L}{\pi\, AR} \qquad (14)$$

The axial velocity at the vortex center and the maximum tangential velocity decrease with the distance behind the wing (Fig. 15) as expected due the simulation results (Fig. 8). The initial value of the axial velocity is influenced by the circulation of the wing and depends, therefore, on the angle of attack. For the chosen case, V_a begins with an excess speed, corresponding to $1.4*V_\infty$, and decreases to an asymptotic value of about $0.8*V_\infty$. For comparison purposes, theoretical values of the asymptotic tangential velocities for an aspect ratio of 4 are taken from Fig. 11, where a maximum of $\bar{V}_t = 2.9$ is found. Substituting this value in Eq. (14), we obtain $V/V_\infty = 0.73$, for $\beta = 0.915$, AR=4 and $C_L = 0.9$ (at an angle of attack of 13°), which is in good agreement with the experiments.

Fig. 16 summarizes the influence of the aspect ratio on the final core radius for rectangular wings. For large aspect ratios, the core radius converges against an asymptotic value of 0.02, while for small aspect ratios the limit is fixed by the value of an elliptical wing (≈0.055). This latter, calculated value is also plotted in Fig. 16 showing again a good agreement between experiments and theory.

In Fig. 17 the measured influence of the angle of attack on core radius and velocity components is shown at a constant distance of x/s=2. The core radius R_c/s was found independent of the angle of attack. This follows, for a given lift distribution, from the Biot-Savart method. It is true that the circulation Γ_0 grows with increasing angles of attack but this only fastens the speed of the roll-up process and does not influence the final structure of the tip vortices. Therefore, the dimensionless tangential velocity $\bar{V}_t$ remains constant and, because of Eq. (14), V_t/V_∞ grows with the lift coefficient and the angle of attack. The axial velocity which has a minimum at the axis of the vortex grows with α. This tendency is due to the larger values of the initial V_a caused by the increasing circulation.

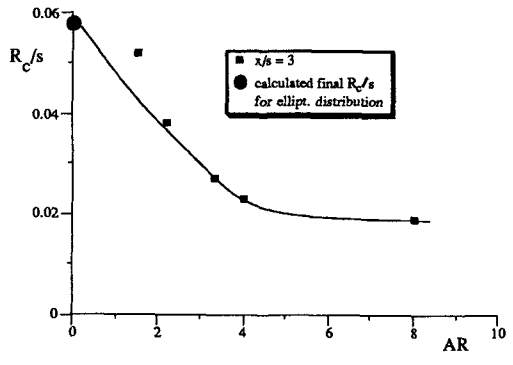

Fig. 16 Core radius as function of aspect ratio

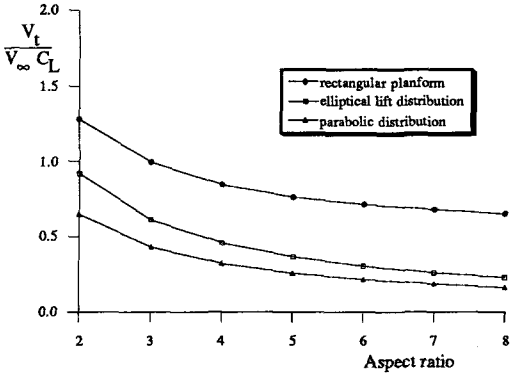

Fig. 18 Comparison of the maximum tangential velocitiy for various lift distributions and wing planforms

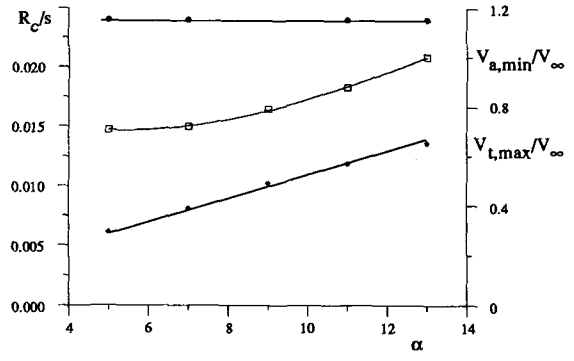

Fig.17 Vortex parameters as functions of angle of attack

Methods of vortex wake alleviation

This section concerns some methods for reducing the maximum of the tangential velocity which is induced by tip vortices. One can distinguish between the influence of lift distribution and tip devices of passive and active type. The experimental investigations of tip devices are focussed on passive means, in particular on the methods of

— destabilizing concentrated vortices
— the breakdown of a vortex core
— inserting a stator in the tip vortex center

The influence of lift distribution on tip vortex strength

The amalgamation method permits the investigation of roll-up for arbitrary lift distributions. The influence of various lift distributions on the maximum tangential velocity was already shown in Fig.12. Applying Eq. (14), the maximum tangential velocity can be related to the free-stream velocity and the lift coefficient for the lift distribution and planforms, presented in Fig. 11. The essential influences are shown in Fig. 18. Smoothing the lift distributions — from rectangular planforms to parabolic distributions — reduces the maximum tangential velocities considerably. A smaller influence is observed if the aspect ratio is increased.

Vortex wake alleviation by tip-devices

To reduce the strength of the tip-vortices, different devices have been tested in an experimental program. In the following section the basic function of these devices will be presented as well as experimental results.

Reduced vortex stability behind spoilers

One method of controlling tip vortices could be the artificial stimulation of vortex instability which may lead to vortex breakdown. In this section a short introduction to stability conditions of vortices is given before results of experiments related to the stability problem are presented. In these experiments the reduction of stability is effected by suitably located spoilers.

For assessing vortex stability, the measured tangential and axial velocity profiles have been approximated analytically. For this purpose, the tangential velocity profile will be described by the Lamb-Oseen model.

$$\frac{V_t(R)}{V_\infty} = \frac{C}{R}\left(1 - e^{-\lambda R^2}\right) \tag{15}$$

while the measured axial velocity profiles are fitted to a Gaussian distribution:

$$\frac{V_a(R)}{V_\infty} = 1 - \delta e^{-\mu R^2} \tag{16}$$

By extracting the parameters C, λ,$\mu$and δ from fitting the experimental results, a good approximation of the vortex structure can be obtained near the vortex center, where, normally, the instability begins.

In the past, criteria for hydrodynamic stability of vortices were published by several authors of which the best known may be the criteria published by Ludwieg [11]. These criteria are based on the equilibrium between pressure forces and centripetal forces in a vortex, the stability of which was already investigated by Rayleigh at the beginning of this century. Ludwieg extended the stability condition by incorporating the influence of axial flow profiles. Since the criterion developed by Leibovich and Stewartson [12] meets the most rigid conditions, it will be used for stability calculations in this paper. As derived

by Staufenbiel and alii [13] using the models of Eqs. (15) and (16), the sufficient condition for vortex instability is given by

$$\frac{q}{\sigma} = \frac{1.57 \cdot V_{t,max}}{\sigma \cdot |\delta| \cdot V_\infty} < \sqrt{2} = 1.4 \qquad (17)$$

if the abbreviations

$$\sigma = \mu/\lambda \qquad \text{and} \qquad q = C\frac{\sqrt{\lambda}}{|\delta|} \qquad (18)$$

are used. Fitting the velocity profiles it was shown in [13] that it is necessary to distinguish different parameters λ and μ in the Lamb and the Gaussian models.

According to the instability condition (17), an enlarged axial velocity defect results in reduced stability. To increase the defect, an experiment was carried out, in which an additional wake of a spoiler penetrated the vortex center. Results will be presented for a rectangular wing planform of aspect ratio AR=4. The spoiler was placed on the wing tip in a part where a high concentration of vorticity is expected. The spoiler position turned out to be a very sensitive parameter for destabilizing the vortex. The test setup is shown in figure 19.

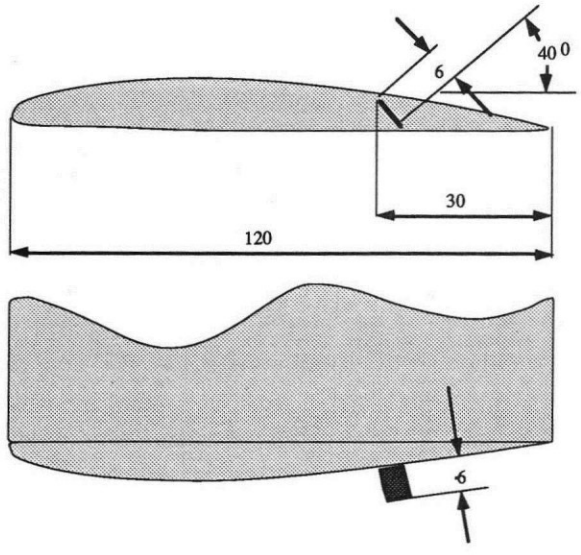

Fig 19 Wing tip configuration and spoiler position

The axial velocity profiles change significantly over a short length in streamwise direction (Fig. 20). From x/s=0.5 to x/s=0.6 the axial velocity decreases rapidly, from $0.9*V_\infty$ to about $0.5*V_\infty$, but does not change significantly further downstream, at x/s=2. At x/s=0.5 a minimum defect of the axial velocity is observed off the center which is moved to the center already at x/s=0.6. Within the investigated range the tangential velocities change only slightly.

Flow visualization experiments reveal that the sudden change in V_a coincides with a widening of the core region where the straight vortex center winds up to a helix with a diameter in the order of the vortex core. Downstream of that point (see arrow), the flow character does not change any more as the photo in Fig. 21 illustrates.

A comparison of the velocity profiles at x/s=2, with and without a spoiler, is given in Fig.22. Beside the large difference in the axial velocity — the defect grows from about 0 to about $0.5*V_\infty$ —, the core radius and the tangential velocity also differ. R_c/s grows from 0.028, without spoiler, to 0.042, with spoiler, and the tangential velocity is reduced by about 20%.

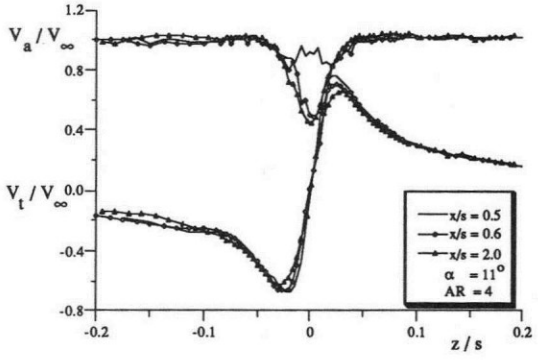

Fig.20 Velocity profiles behind a configuration with spoiler

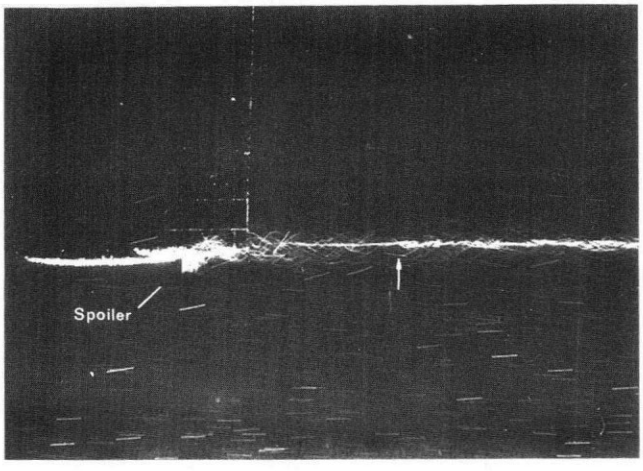

Fig 21 Spiraling of vortex behind a spoiler configuration

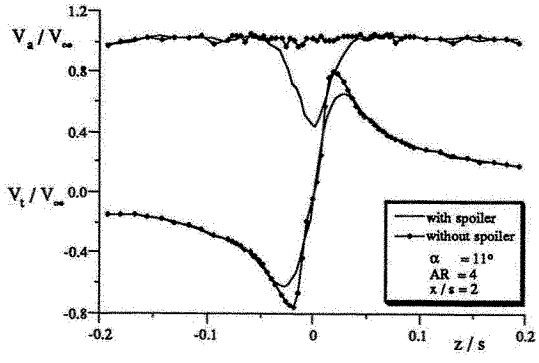

Fig. 22 Velocities behind configurations with and without spoiler

Evaluating the stability parameter at x/s=0.6 gives $q/\sigma=1.63$, a value which comes close to the stability boundary of 1.42. Further downstream, at x/s=2, the vortex is unstable, corresponding to $q/\sigma=1.32$. Thus, it can be concluded that the change in the flow behavior, observed in Fig. 21, is caused by a destabilizing mechanism induced by the additional wake of the spoiler. Even though q/σ falls below the stability boundary, vortex breakdown does not appear as expected. Leibovich and Stewartson [12] have shown that instability implies that an infinite number of modes has a finite growth rate. This suggests that Eq. (17) may be considered as a criterion for "massive instability and transition to turbulence" [14], which are understood as other words for "breakdown". As already shown in [13] and confirmed by our experiments, hydrodynamic instability is not sufficient for the development of vortex breakdown.

For a further reduction of the axial velocity at the vortex center, the bottom and top walls of the water tunnel were inclined by about 4^0 resulting in a diffusor behind the wing. As a result, the diffusor reduces the axial velocity further, to approximately $0.35*V_{l\infty}$, where $V_{l\infty}$ is the locally variing free-stream velocity measured outside the vortex (Fig. 23). In this case, the stability parameter q/σ is reduced down to 1.15 indicating a significant instability.

Again, flow visualization showed that the center of the vortex winds up to a spiral with an increasing spiral diameter. This corresponds to the continuous decrease of the maximum tangential velocity to be taken from Fig. 23. Even though the investigations on this topic are not yet finished, we believe it is fair to assume that hydrodynamic instability must not be turned into a drastic change of the flow pattern in any case but may also show an only modestly disturbed vortex core resulting in continuously varying velocity profiles.

As is well known from delta-wings at high angle of attack, leading edge vortices can break down very closely behind or even above the wing. In general, this type of vortex breakdown is combined with a drastic change of the flow pattern, V_t decreases remarkably and the deficit of V_a increases. Now, the question arises whether it is also possible to stimulate vortex breakdown at tip vortices of non-delta wings. For this purpose a specially shaped wing tip, a half-delta wing tip, has been investigated in the water tunnel. Top and front views of the half-delta tip and its connection to the wing are shown in Fig. 24, in addition to a reference wing tip. In both cases the wing has a rectangular planform with a Clark-Y airfoil. The half-delta is a sharp edged plate which continues the flat lower side of the wing profile. This configuration leads to a stepwise negative aerodynamic twist of 3 degrees at the kink which is slightly rounded off.

In addition, Fig. 24 shows a reference configuration with the same span width. The airfoil of the inner wing is continued to the tip and tapered without any twist but with the same chord distribution as the half-delta; leading and trailing edges are equally swept rearward and forward respectively.

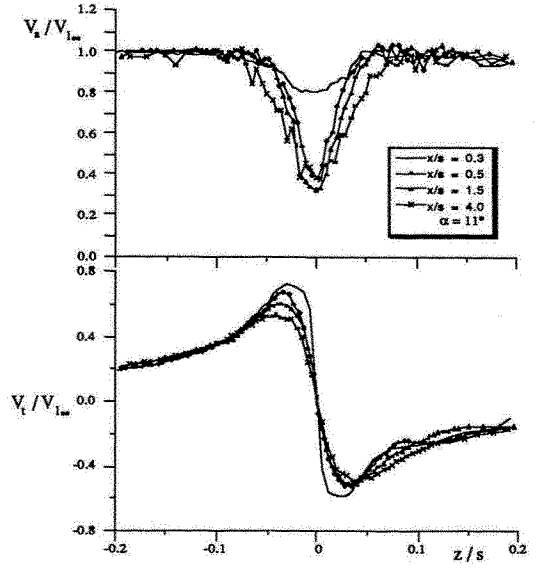

Fig. 23 Velocities behind spoiler configuration in diffusor Half-Delta wing tip

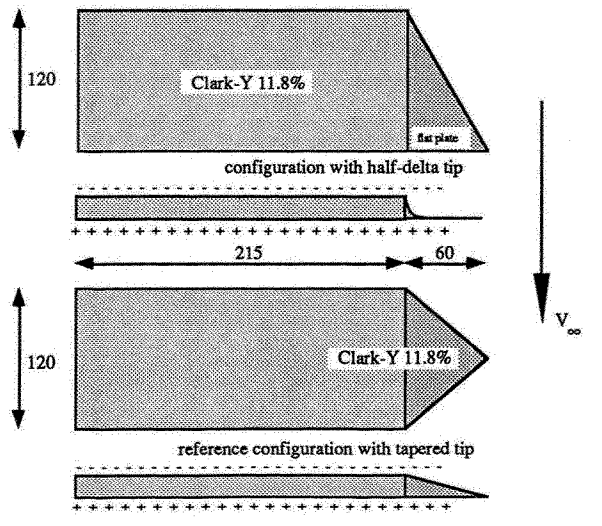

Fig.24 Half-delta and reference wing tips

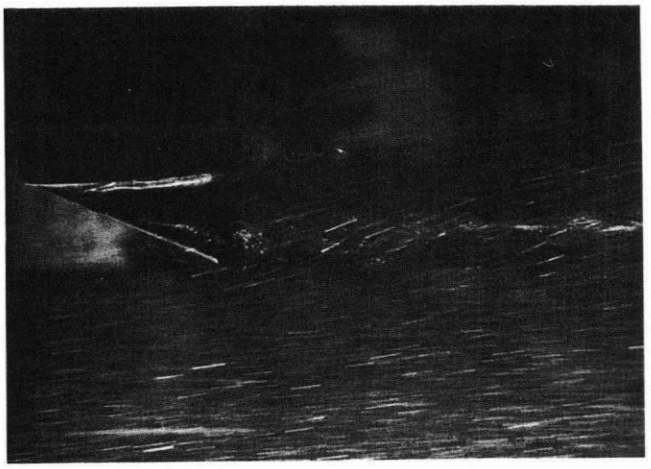

Fig.25 Leading edge vortex at half delta tip

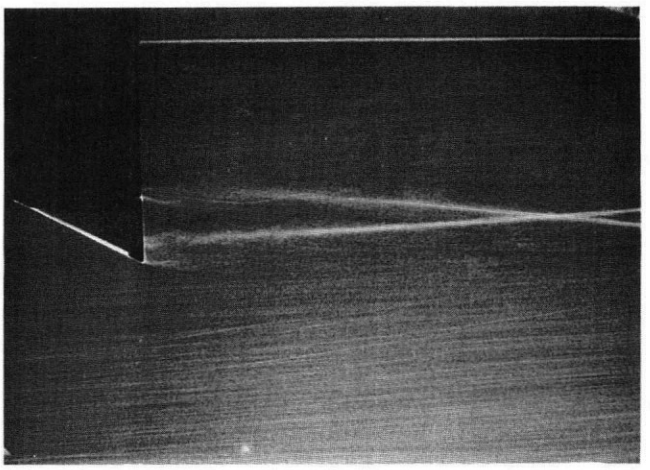

Fig. 27 Two equally strong vortices with half delta tip

It was found, that the half-delta configuration with an aspect ratio of 5 generates a leading edge vortex as a regular delta wing does. But, at the same angle of attack, the leading edge vortex is stronger at the half-delta and breaks down earlier because lift coefficient and circulation are larger at a given angle of attack.

The photograph (Fig. 25) indicates, that, at an angle of attack of $\alpha=13$, a concentrated leading edge vortex breaks down at approximately the half chord position. Some chord lengths behind the wing the vorticity seems to concentrate again. Corresponding velocity profiles are given in Fig. 26.

The reference wing generates a narrow and deep velocity defect down to $V_a=0.6*V_\infty$ while the maximum tangential velocity amounts to $V_{t,max}=0.58*V_\infty$ with a core radius of $R_c/s=0.016$. At the half-delta configuration, the velocity profiles and the core radius are remarkably different from the reference case. The core radius has grown to $R_c/s=0.044$ while $V_{t,max}$ decreases to $0.38*V_\infty$. Thus, $V_{t,max}$ is reduced by about 35%, related to the reference case.

At smaller angles of attack, the half-delta configuration reveals another alleviating effect. In this case, breakdown of the half-delta vortex does not occur any longer but two nearly equally strong vortices roll up, one at the kink of the half-delta and another one at the leading edge (see photograph of Fig. 27).

Axial and tangential velocity profiles are measured downstream at distance of $x/s=2$ where the LDV measuring trace cuts both vortex centers (Fig. 28).

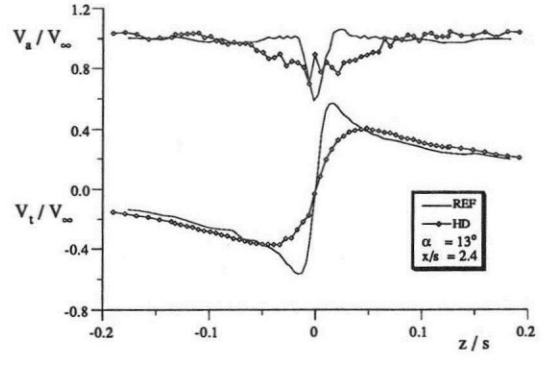

Fig 26 Velocities behind half delta tip and reference wing

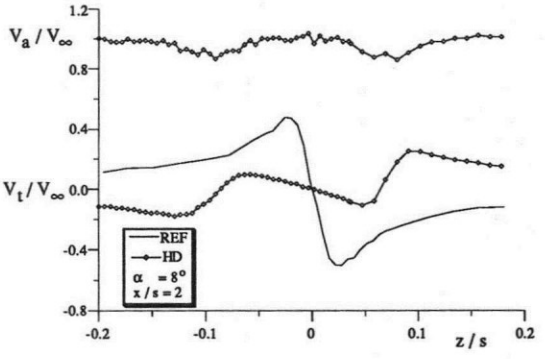

Fig 28 Velocities behind half delta configuration and rectangular wing

For comparison purposes, the tangential velocity profile of the tip vortex of a rectangular wing with a simply rounded tip (without the tapered wing section) is also shown in Fig. 28. Compared to this reference case, the half-delta configuration reduces $V_{t,max}$ even more, to about 50%. This effect is not yet systematically examined but it seems to be worth spending some more research effort on it in the future.

Stator located in the wing tip vortex

Very promising devices to reduce the high tangential velocities in concentrated vortices are rotors or stators located in the vortex centers behind the wing. By properly designing these configurations even a reduction of drag could be achieved.

In principle, rotors or stators in a vortex field redistribute the vorticity concentrated in the tip vortices. Behind a wing tip, the flow can be deviated in such a way that some of the energy of the tip-vortex, contained in the tangential velocity component, is recovered. This change in flow direction leads to a reaction force on the blades which, in general, reduces the resultant drag. A simple model illustrates this effect. Assuming that the vorticity, concentrated in the wing tip vortex, is transferred to the tip vortices of rotor or stator blades and spread over a cylindrical ring with the radius of the blades. Then, the induced drag can easily be calculated using the Kirchhoff-Routh function. The result of this calculation is summarized in Fig. 29 showing a considerable reduction of the induced drag with increasing values of the ring radius a.

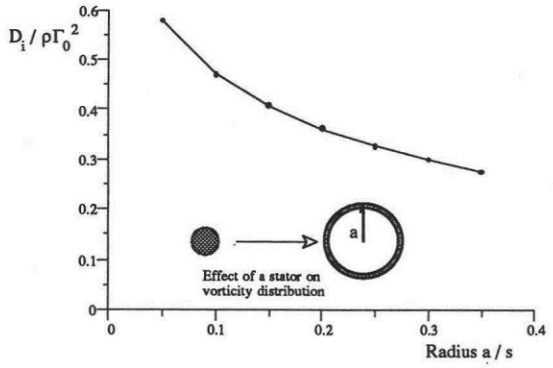

Fig. 29 Effect of spreading the vorticity distribution

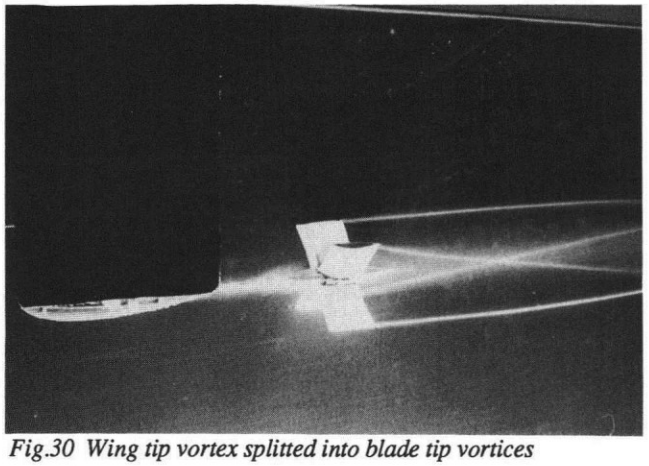

Fig.30 Wing tip vortex splitted into blade tip vortices

In the following, we confine the investigations to the effect of a stator. The redistribution of wing vorticity by a stator may be described as follows. The vorticity in the wing wake is assumed to be highly concentrated so that the inflow to the stator has a strong rotational component. If the design of the stator, consisting of a hub and a number of blades, is properly adapted to the rotational flow field, it experiences forces leading to blade tip vortices which transfer vorticity from the wing tip vortex to the blade tip vortices (Fig 30). The strength of these vortices depends on the design and the number of blades.

For the estimation of the stator´s influence on the maximum tangential velocity, we consider an optimized stator with four rectangular blades of AR=1 and assume that half of the vorticity of the wing wake, Γ_0, remains concentrated in the wing tip vortex, while the other half should be distributed over the blades with a strength of 0.12 Γ_0 per blade. As presented in the last section (Fig.16) for rectangular wings, the core-radius of rectangular stator blade vortices is derived as $(R_c/a)_s=0.05$ for an aspect ratio of AR=1, while the core radius of the wing-tip vortex is given by $(R_c/s)_w=0.025$ for AR=5. The ratio of the wing half span s and the radius of the blades a is chosen equal to the value of the test configuration, (s/a)=9.1. By combining these terms, the ratio of the core radii of wing and stator tips is given by

$$r_c = \frac{R_{cw}}{R_{cs}} = \frac{R_{cw}/s}{R_{cs}/a}\,\frac{s}{a} = 4.5 \qquad (19)$$

This value leads to a stator-induced reduction of the maximum tangential velocity according to

$$\frac{V_{ts}}{V_{tw}} = r_c\,\frac{\Gamma_{os}}{\Gamma_{ow}} = 4.5*0.12 = 0.54 \qquad (20)$$

This reduction depends mainly on the aspect ratio of the blades. At constant stator span widths, a decreasing aspect ratio results in a growing core-radius so that r_c and the maximum tangential velocity are reduced. Furthermore, the partition between the vorticity left to the wing vortex and transferred to the blade tip vortices can be optimized further than done in this study.

The side-effect of a stator, the reduction of the induced drag, is illustrated in Fig. 31. Because of the inclined flow direction, the lift vector L is tilted forward and yields an induced thrust component. If the tangential velocity component of the vortex is large enough, the induced thrust may be sufficient to overcompensate the additional profile drag, D_s, of the stator and a thrust component, F_x results.

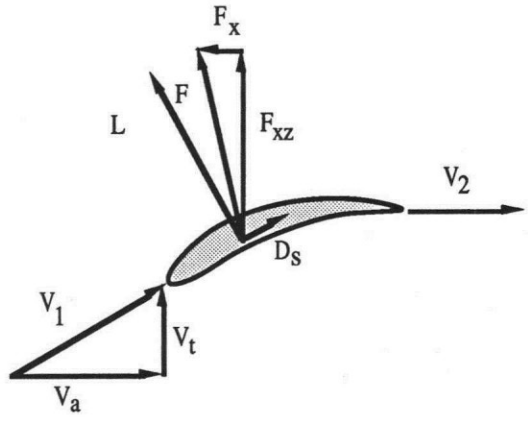

Fig.31 Force and velocity vectors at stator blade

Thus, an effective stator, suitable for operational use, has to be designed for a minimization of the tangential velocity component in the flow behind the stator, with the constraint, that no increase of the total drag of the wing-stator configuration should occur. In order to obtain acceptable dimensions, the maximum stator diameter was limited to about the chord-length of the wing. It has been found in the design process that, for a rectangular wing planform, a smaller diameter was sufficient. For several reasons a lowering of the aspect ratio of the blades is advantageous:

— it leads to a larger core radius of the blade tip vortices and, thus, to lower tangential velocities,
— the structural weight of the stator is decreased,
— the friction is smaller due to higher Re-number.

The inflow to the stator of the test configuration was measured by a LDV and could be considered as a known condition. For transferring vorticity from the center of the wing tip vortex, the stator blades had to turn the direction of the flow in such a way that the tangential velocity is reduced as much as possible behind the blades while producing a minimum of additional profile drag. This condition requires aerodynamically twisted blades because of the variation of the tangential velocity component in radial direction. The profiles, used in the test configuration, varied from a NACA 65-(15)10 (hub) over a 65-809.6 to a 65-409 NACA-profile at the tip.

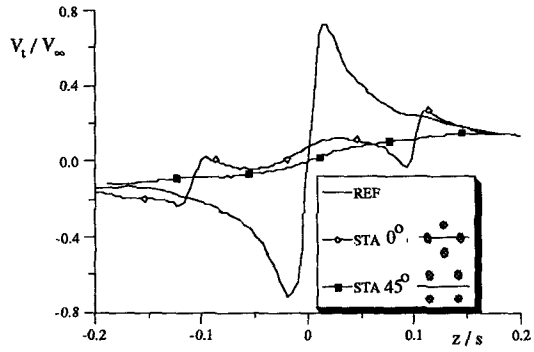

Fig.32 Velocities behind a stator and a rectangular wing

Results for the test configuration, obtained by LDV measurements in the water tunnel, are shown in Fig. 32. Here, the flow fields behind the clean configuration and downstream of a four bladed stator are compared. In the latter case, axial and tangential velocity components were measured along two different lines. The largest values of V_t are obtained along a line which cuts two of the blade tip vortices (marked as 0 degree) while a smoothed profile is measured along the 45-degree line. In the clean configuration the value of $V_{t,max}$ is about five times as high as it is downstream of the stator. The measurement on the 45-degree line represents the velocities induced by the remaining vorticity of the wing tip vortex since the induction of the four blade tip vortices adds to zero on this line because of the antisymmetry of the blade tip vortices. The scattering of the measurements of the axial velocity (not plotted) indicates that the level of turbulence is raised by the presence of the stator which may, in addition, lead to a faster ageing process.

In addition to the velocity measurements, forces and pitching momentum were measured in the water tunnel, using a five-component strain gage balance, to investigate the performance of different configurations. For the configuration described above, the total drag is reduced by about 7% at constant lift.

For assessing the efficiency of wake vortex alleviation methods, it is not so much the maximum tangential velocity which is of interest as the rolling moments imposed on vortex encountering aircraft. For the optimized stator configuration, an estimate of the rolling moments will be given now, based on the following assumptions: diameter of the stator =0.1 s_g; span widths ratio of the vortex generating and the encountering aircraft $s_g/s_e=5$; velocity ratio $V_g/V_e=2$. For two relative positions between encountering wing and stator wing tip vortices (see Fig. 32), the coefficient of the rolling moment is determined, using the equation

$$C_l = (1/s^2) \int_{-s}^{s} \frac{dC_L}{d\alpha} \frac{V_t(y)}{V_\infty} y \, dy, \qquad (21)$$

and is presented in the following table

Statorless	with Stator (0^0-Position)	with Stator (45^0-Position)
0.256	0.182	0.097

Thus, using a stator configuration, the rolling moment for an encountering aircraft are reduced by 30% and 63%, for the given example. This result depends on the position of the stator tip vortices relative to the wing, on the diameter of the stator and the span of the following aircraft. In addition, nonlinear effects in the influence of angle of attack α on lift coefficient and on local flow separation have to be considered because of the large induced angles of attack.

Concluding remarks

In the first part of this paper, investigations on the formation and structure of wing tip vortices are presented. A computational method for the time-dependent roll-up process is derived, which is based on the Biot-Savart approach with a particular technique of amalgamation which preserves energy, center of vorticity and the second moment of vorticity distribution. The results are proved by various experiments performed in a water tunnel. The roll-up process is characterized by three phenomena

- — the core radius grows,
- — the maximum tangential velocity decreases even though the circulation in the vortex grows,
- — the axial velocity at the center of the vortex is considerably reduced.

The second part of the paper is focused on devices for vortex wake alleviation which apply the three methods of

- — artificially destabilizing the vortex,
- — inducing breakdown of the vortex core and
- — spreading the vorticity by a stator located in the wing tip region

The methods, examined experimentally in a water tunnel, resulted in a remarkable reduction of the tangential velocity which also provides an essential reduction of the rolling moments imposed on a vortex encountering aircraft. As particularly promising was a stator configuration found, which not only reduces the vortex strength considerably but also leads to a decrease in the total drag of the wing-stator combination.

Acknowledgements

This research has been supported by the 'Deutsche Forschungsgemeinschaft (DFG)' under the Special Research Program 'Wirbelsysteme in der Flugtechnik' (SFB 25). The authors are grateful to Dr.-Ing D. Coors for valuable discussions and to Dipl.-Ing S. Fell who was helpful at performing the numerical calculations.

Literature

1 Bilanin, A.J. and Donaldson, D. du P.: Estimation of velocities and roll-up in aircraft vortex wakes, J. Aircraft, Vol.12, 1975, pp.578-585

2 Ciffone, D.L. and Orloff, K.L.: Far-field wake-vortex characteristics of wings, J. Aircraft 12, 1975, pp. 464-470

3 Corsiglia, V.R., Rossow, V.J. and Ciffone, D.L.: Experimental study of the effect of span loading on aircraft wakes, J. Aircraft, Vol.13, No.12, 1976, pp. 968-973

4 Moore, D.W.: A numerical study of the roll-up of a finite vortex sheet, J. Fluid Mech., Vol. 63 part 2, 1974, pp. 225-235

5 Saffman, P.G.: The structure and decay of trailing vortices, Arch. Mech., Vol.26, 1974, pp.423-439

6 Spreiter, J.R. and Sacks, A.H.: The rolling up to the trailing vortex sheet and its effect on the downwash behind wings, J. Aeron. Sci. 18, 1951, pp. 21-32

7 Staufenbiel, R.: Structure of Lift-Generated Rolled-up Vortices, Journal of Aircraft, Vol 21, 1984, pp. 737-744

8 Staufenbiel, R. : Ein Modell zur analytischen Beschreibung von Randwirbeln, Z. Flugwiss. u. Weltraumforsch., (ZFW), 1985, Nr. 9, Heft 5

9 Sarpkaya, T.: Computational Methods with Vortices - The 1988 Freeman Scholar Lecture, Journ. of. Fluids Engineering, Vol. 111, March 1989, pp. 5-52

10 Staufenbiel, R. and Scherer, Th.: Ein modifiziertes Punktwirbelverfahren zur Beschreibung des Aufrollvorgangs bei Randwirbeln, submitted to Z. Flugwiss. u. Weltraumforsch. (ZFW), 1988,

11 Ludwieg, H.: Stabilität der Strömung in einem zylindrischen Ringraum, und Ergänzungen zur Arbeit, Z. Flugwiss. 8, 1960, pp. 135-140 und 9, 1961, pp.359-361

12 Leibovich, S. and Stewardson,K.: A Sufficient Condition for the Instability of Columnar Vortices, J. Fluid Mechanics, Vol.126, 1983, pp.335-356

13 Staufenbiel, R., Helming,T., Vitting, T.: Controlled breakdown of tip vortices, Proceed. of the *Colloquium on Vortex Breakdown*, Baden, Schweiz, 1987, pp.95-114

14 Leibovich, S.: Vortex Stability and Breakdown: Survey and Extension, AIAA Journal, Vol. 22, Sept. 1984, pp. 1192-1206